

Article

Streams with Riparian Forest Buffers versus Impoundments Differ in Discharge and DOM Characteristics for Pasture Catchments in Southern Amazonia

Higo J. Dalmagro ¹, Michael J. Lathuillière ^{2,*}, Fernando da S. Sallo ¹, Maurel F. Guerreiro ¹, Osvaldo B. Pinto Jr. ¹, Paulo H.Z. de Arruda ³, Eduardo G. Couto ⁴ and Mark S. Johnson ^{5,6}

¹ Programa de Pós-Graduação em Ciências Ambiental, Universidade de Cuiabá, Cuiabá, Mato Grosso 78.025-300, Brazil; higojdalmagro@gmail.com (H.J.D.); fdss88@gmail.com (F.d.S.S.); maurel.guerreiro@hotmail.com (M.F.G.); osvaldo.borges@gmail.com (O.B.P.J.)

² Stockholm Environment Institute, Stockholm 10451, Sweden

³ Programa de Pós-Graduação em Física Ambiental, Universidade Federal de Mato Grosso (UFMT), Cuiabá, Mato Grosso 78060-900, Brazil; paulo.zanella@gmail.com

⁴ Departamento de Solos e Engenharia Rural, Faculdade de Agronomia, Medicina Veterinária e Zootecnia, Universidade Federal de Mato Grosso, Cuiabá, Mato Grosso 78060-900, Brazil; egcouto@gmail.com

⁵ Institute for Resources, Environment and Sustainability, University of British Columbia Vancouver, BC V6T 1Z4, Canada; mark.johnson@ubc.ca

⁶ Department of Earth, Ocean and Atmospheric Sciences, University of British Columbia Vancouver, BC V6T 1Z4, Canada

* Correspondence: michael.lathuilliere@sei.org; Tel.: +46 73 707 8583

Received: 14 January 2019; Accepted: 19 February 2019; Published: 23 February 2019



Abstract: Forest to pasture land use change following deforestation in Southern Amazonia can result in changes to stream water quality. However, some pasture streams have riparian forest buffers, while others are dammed for farm ponds. Stream corridor management can have differential effects on hydrology and dissolved organic matter (DOM) characteristics. We examined rainfall-runoff patterns and DOM characteristics in a pasture catchment with a forested riparian buffer, and an adjacent catchment with an impoundment. Total streamflow was 1.5 times higher with the riparian buffer, whereas stormflow represented 20% of total discharge for the dammed stream versus 13% with buffer. Stream corridor management was also the primary factor related to DOM characteristics. In the impounded catchment, DOM was found to be less structurally complex, with lower molecular weight compounds, a lesser degree of humification, and a larger proportion of protein-like DOM. In the catchment with a forested buffer, DOM was dominated by humic-like components, with fluorescence characteristics indicative of DOM derived from humified soil organic matter under native vegetation. Our results suggest that differences in stream corridor management can have important implications for carbon cycling in headwater pasture catchments, and that such changes may have the potential to influence water quality downstream in the Amazon basin.

Keywords: pasture; land use change; Amazon; fluorescence spectroscopy; dissolved organic carbon

1. Introduction

The Amazon basin plays a significant role in the global carbon (C) cycle [1]. The basin contains a variety of landscapes spanning from pristine forest to regions impacted by deforestation and fires resulting from agricultural expansion [2]. Since the 1970s, agricultural land expansion and intensification have been changing the landscape of Southern Amazonia through the replacement of

native forests with pasture or cropland [3]. In Brazil, net forest loss in the "arc of deforestation" between 1990 and 2015 accounted for 41% of global forest loss during those years (53 out of 129 Mha) [4,5]. Mato Grosso emerged as the state with the highest rate of deforestation between 1988 and 2018 with a total loss of 14.3 Mha (33.1% of the total Brazilian deforestation) [6]. For decades, the predominant land cover following deforestation has been pasture for livestock, with more recent conversions directly to cropland or from pasture to cropland [7,8]. These changes in land use have had a number of consequences on freshwater ecosystems, especially with respect to hydrology and biogeochemistry of small streams [9–11].

Dissolved organic matter (DOM) enters inland waters in response to various natural factors (e.g., climate and landscape), anthropogenic forcings (e.g., land use), as well as hydrological processes [12–15]. Several studies show that the quantity and quality of DOC is proportional to land cover type [16,17], though few studies have evaluated the influence of stream corridor management following catchment-scale land cover change. Land use change impacts the hydrology of headwaters stream characteristics in ways that may influence DOM delivery and transformation [18–20] since the quantity and quality of DOM is controlled by biological (e.g., primary production and decomposition), chemical (e.g., photodegradation and redox reactions), and physical processes (e.g., hydrology) [15,21–23]. DOM in aqueous systems is a heterogeneous mixture of organic compounds that have ecologically important functions in processes that impact the C cycle and nutrient cycling [24]. Although organic matter can be rapidly degraded by biological activities, its chemical and fluorescence characteristics allow for the use of DOM concentrations and characterization as an environmental tracer in some ecosystems [25,26]. While land use change at the catchment scale has been evaluated relative to hydrology and water quality in streams [20,27], the influence of stream corridor management (e.g., the presence or absence of riparian buffers, or the presence or absence of reservoirs or impoundments) on hydrological functioning and stream water quality has received little attention by researchers.

Analysis of excitation emission matrices (EEMs) of water samples via fluorescence spectroscopy allows for a detailed view of DOM characteristics in environmental samples. EEMs can be used to track the origins of individual DOM peaks observed in aqueous samples [28], aiding in the identification of C origin. Thus, monitoring of DOM dynamics provides substantial information about the connections and ecosystem functioning in space and time [13,14,29,30]. Recently, fluorescence and optical absorbance techniques have been used to assess water quality in agricultural river basins [26], as well as Brazilian basins that cover tropical savannah (e.g., Cerrado), wetland (e.g., Pantanal), and urban areas [16]. Fluorescence characterization facilitates the detection of differences between natural and anthropogenic sources of DOM in agricultural streams [31]. Thus, a combination of optical properties (fluorescence and absorption) in conjunction with conventional DOC measurements can be used to discriminate temporal and spatial variations of DOM.

This study aims to evaluate hydrological dynamics and the DOC quantity and DOM quality for adjacent pasture catchments with differing stream corridor management in Southern Amazonia to better understand the influence of stream corridors on hydrology and C cycling in different hydrological periods. Results provide additional evidence for a better assessment of the role of headwater streams in the C cycle following deforestation events.

2. Materials and Methods

2.1. Site Description and Headwater Watersheds

The study was carried out at the Pedra Alta ranch in the municipality of Alta Floresta, Mato Grosso, Brazil, located in Southern Amazonia. The Pedra Alta ranch (9°49' S, 55°59' W, 300 m.a.s.l.) is located near the southern slopes of the Serra do Cachimbo in the lower part of the Teles Pires river basin [32] (Figure 1). This 2000 ha ranch was established in 1983 and has 1450 ha of pasture (*Brachiaria* genus) with low application of mineral fertilizers and 550 ha of forest. The predominant soil at the ranch is classified as Chromic Acrisol [33] with 784 g kg⁻¹ of sand, 80 g kg⁻¹ of silt and 136 g kg⁻¹

of clay, 15 g kg^{-1} total nitrogen, 138 g kg^{-1} of organic carbon (0–0.10 m depth), and a soil pH of 5.3 (in 1:2.5 soil:water slurry). The tropical forest vegetation consists of dense evergreen species with an average height of 30 m, but with some emergent trees reaching a height of up to 45 m [34]. The 30-year mean annual temperature is $25.7 \text{ }^{\circ}\text{C}$ with a mean annual precipitation of 2230 mm y^{-1} distributed over a pronounced dry season (June to September, 230 mm) and wet season (October to May, 2000 mm) [32].

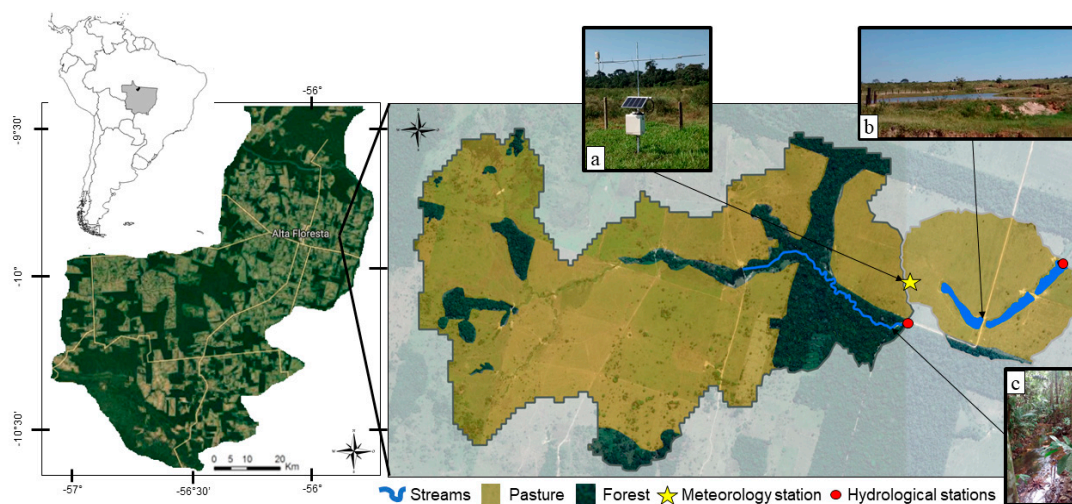


Figure 1. The location of the Pedra Alta ranch in Alta Floresta, Mato Grosso, Brazil, in Southern Amazonia with the location of the micrometeorological station (yellow star (a)) and the two studied headwater pasture catchments (Dam (b), and Forest (c)). Water samples were collected and discharge recorded at locations indicated by red circles.

We selected two headwater pasture catchments, one with riparian forest adjacent to streams (e.g., riparian buffer) and the other with a dammed stream (Figure 1). The catchment with the dammed stream without riparian forest buffer was classified as a first-order catchment of 59 ha (hereafter known as the “Dam catchment”), with a series of three impoundments used for drinking water for livestock. These reservoirs are representative of typical small reservoirs (i.e., farm ponds) commonly established when pastures are cleared from forested ecosystems in this region of the Amazon [10] (Figure 1). The catchment with forested riparian buffer (hereafter the “Forest catchment”) is a 360 ha second order catchment. This catchment presented a mix of land covers: 62 ha of forest buffering the streams in which we collected water samples; 298 ha under pasture (Figure 1).

The catchment boundaries were delineated by interpolating between contours established with a high-precision differential GPS (Hiper+, Tocon Inc., Tokyo, Japan) with relative altitudes georeferenced to altitude reported in Google Earth. In addition, GPS data was used to calculate the slope angle of the water bodies. We measured the vertical distance as the difference in elevation between collection points and the horizontal distance calculated as the pathlength between collection points. We took the arc tangent of the relationship between the vertical distance and the horizontal distance to define the stream slope for each catchment.

2.2. Precipitation and Discharge Measurements

Precipitation and discharge were monitored over 15 months every 10 min between 15 May 2016 and 28 August 2017. Precipitation and rainfall intensity were measured with a meteorological station (WXT520, Vaisala Inc., Helsinki, Finland, accuracy $\pm 5\%$) installed between the two catchments (Figure 1) and connected to a CR1000 datalogger (Campbell Scientific Inc., Logan, UT, USA). Discharge was measured in both catchments using a water level sensor (CTD-10, Decagon Devices, Inc., Pullman, WA, USA, $\pm 0.05\%$ complete scale at $20 \text{ }^{\circ}\text{C}$) coupled to a small microcontroller (Arduino UNO R3, <https://www.arduino.cc>) combined with a standard Arduino SD protection card for data storage [35].

The sensors were installed in the base of the main stream thalweg and protected inside a perforated PVC tube. The tube and sensor were protected against roots and trees along the flow bank for stability during storm flows. We also performed water level measurements during field visits using a tape measure (± 0.01 m) to validate the sensor measurements.

We developed flow classification curves based on flow discharge measurements performed on 28 December 2016, 7 March 2017, 30 April 2017, 27 August 2017, and 30 December 2017. These measurements covered the range of minimum to maximum stages of the baseflow. The calculation of the instantaneous flow discharge was made from measurements of the cross-section of the fluvial channel at the flow sampling points [36] and the stream velocity of both watersheds. Flow velocity was measured using a fluvimetric micromoline (model MCN-1, Inc., Belford Roxo, NJ, Brazil). We used power adjustments to define stage-discharge curves with resulting power functions for the Dam catchment ($Q_d = 2.27 \times 10^{-13} WL^{4.407}$, $R^2 = 0.96$), where WL is the water level, and Q_d is the discharge, and the Forest catchment ($Q_f = 7.55 \times 10^{-6} WL^{1.829}$, $R^2 = 0.85$), where Q_f is the discharge (Figure S1).

Using this information, we calculated daily discharge based on the automatic water level measurements normalizing discharge by the watershed area (mm d^{-1}). We then separated the hydrographs into baseflow and stormflow components. The contribution of baseflow to total discharge was estimated by the baseflow index calculated by hydrograph separation using a digital filter implemented by Ladson et al. [37] that takes into account the algorithm Lyne and Hollick [38]. Stormflow was obtained as the difference between total discharge and baseflow. We present baseflow and stormflow as a percentage of total stream discharge.

2.3. Water Sampling and Processing and Environment Variables Measurements

Streamwater samples were collected in both Dam and Forest catchments on five occasions (25 July 2016, 5 November 2016, 7 March 2017, 29 April 2017, and 28 August 2017). These dates covered a range of flow levels and antecedent precipitation levels. We collected 11 sampling points in the Dam catchment located along the stream, and 15 sampling points in the Forest catchment (Figure 1). At each sampling points (distant 50 m from one point to the other), we obtained a sample 0.10 m below the surface from visually well mixed sites in the main thalweg. Water samples were filtered in the field using pre-combusted filters (Whatman GF/F glass fiber filter, 0.7 μm pore size) prior to being stored in 60 mL amber glass vials with Teflon-lined tops previously acid washed [16,39]. Water samples were refrigerated (about 6 $^{\circ}\text{C}$) and stored in the dark for laboratory testing within 24 hours of collection.

For each sampling location, we also measured pH, oxidation-reduction potential (ORP, mV) and stream temperature (T_w , $^{\circ}\text{C}$). These measurements were made using a portable HI 98121 (Hanna Instruments, Woonsocket, RI, USA). Corrections in ORP were made based on the water temperature at each collection point following [40] as shown in Equation (1):

$$E_h = \text{ORP} - 0.6743 T_w + 273.76 \quad (1)$$

where E_h (mV) is the corrected oxidation-reduction potential [39,41].

2.4. Measurements of DOC and Characterization of DOM Compositions

Water samples were divided into two aliquots. The first aliquot was used for DOC concentration measurements which were determined by UV-Vis absorbance using a spectrophotometer (Spectro::lyser®-S::can MESSTECHNIK GmbH, Vienna, Austria, precision $\pm 2\%$) with absorbance measured between 200 and 750 nm in increments of 2.5 nm and with results referenced to a blank spectrum derived from 18.2 M Ω Milli-Q ultrapure water. Measurements of DOC concentration were corrected using a calibration curve developed by preparing solutions of DOC concentrations known from standards obtained from the International Humic Substances Society (IHSS) [16,39]. Previous studies have found similar relationships between DOC means derived from the spectrophotometer

and those determined by the combustion techniques in a TOC analyzer (Multi NC3100e, Jena Analytik AG, Germany) [39,42]. However, the TOC analyzer was out of service during the present study. DOC concentration estimates were corrected from the Spectrolyser default values (i.e., DOC derived using scan global calibration) using the calibration curve developed using the IHSS SWHA standards (Figure S2) and compared with previous calibration curves developed using the Jena Analytik TOC. The IHSS-derived and Jena Analytik TOC-derived estimates differed by < 5% overall for the full sample set. The DOC values in this study are reported based can be considered internally consistent (e.g., for comparing between the two catchments). The reported DOC values have an estimated error of $\pm 10\%$.

The second aliquot was used to generate the excitation-emission matrices (EEMs) using an Aqualog fluorescence spectrometer (Horiba Scientific, Edison, NJ, USA) with a quartz cuvette of 1 cm path length and excitation wavelengths (Ex) between 240 and 600 nm at 3 nm intervals, and emission wavelengths (Em) between 213 and 621 nm at 3.1 nm interval, (and pass = 3 nm, integration time = 1 s). In total, 130 EEMs were measured: 55 EEMs for the dam catchment and 75 EEMs for the forest catchment.

2.5. EEMs Pre-Processing and Parallel Factor Analysis (PARAFAC)

EEMs from the Dam and Forest catchments were analyzed together by PARAFAC [43] to increase the variability of DOM fluorescence signatures and help detect components that might otherwise be present in insufficient amounts to be detected in our study area [44]. Preprocessing prior to applying PARAFAC was performed using the eemR package (version 0.1.4) in R (v.3.1.3) [45] to visually evaluate identify and exclude samples that presented analytically compromised EEMs. Of the 130 water samples collected in the two catchments, only three were excluded due to apparent analytical artifacts in the unprocessed EEMs. Following this screening, correction factors were applied in the remaining EEMs, including the removal of the first and second order Raman scattering, absorbance corrections and internal filter effects, blank subtraction, and standardization for Raman units. For the latter, EEMs were normalized using the integrated fluorescence intensities for a DOM-free water standard evaluated daily under maximum fluorescence intensity [46]. After the pre-processing steps, a file containing the corrected EEMs was generated and used to develop the PARAFAC model in MATLAB (MathWorks, Natick, MA, USA) using drEEM and the N-way toolbox [43].

The analysis of PARAFAC using the split-half validation technique of Stedmon and Bro [47] yielded a three-component model (C1–C3) that explained 99% of the total variation in the fluorescence EEMs dataset of the samples collected in the study catchments. The peak excitation and emission wavelengths for each component were then compared with components reported in the literature and registered in the Openfluor database [48].

2.6. Optical Indices Calculations

We calculated four optical indices representing DOM characteristics, with three calculated from the EEMs including the fluorescence index (FI), humification index (HIX) and biological index (BIX) using the R package eemR version 0.1.4 [45], while the data extracted from the scan UV-Vis sensor was used to calculate slope ratio (SR) [16].

FI represents the ratio between the maximum fluorescence emission intensity at 470 nm and 520 nm, excited at 370 nm [49], has been used to distinguish between DOM of terrestrial, or allochthonous, versus microbial, or autochthonous, origins [50,51]. FI values between 1.2 and 1.5 are indicative of terrestrially derived DOM [51]. HIX values are calculated by dividing the integrated fluorescence intensity between 435 and 480 nm emission wavelength with excitation at 254 nm by the integrated fluorescence intensity between 300 and 345 nm emission wavelength with excitation at 254 nm [52] and is used as an indicator of a material's age and recalcitrance within a natural system [53,54]. Low (<5) values for HIX have been found to correspond to fresh DOM derived from plant biomass and animal manure [55–57], while higher values correspond to DOM that is generally

resistant to degradation and should persist in the environment longer than substances with lower degrees of humification [56,58]. The BIX ratio is calculated by dividing the emission intensity at 380 nm by the maximum emission intensity observed between 420 and 435 nm, obtained at excitations 310 nm [59]. BIX values between 0.8 and 1.0 correspond to DOM of a microbial origin, whereas values < 0.6 are considered to be derived from allochthonous DOM sources [58]. Finally, the spectral slope ratio (SR) was calculated as the ratio of the slopes of the absorbance spectra over 275–295 nm and 350–400 nm segments, where the spectral slope for each segment was calculated using a nonlinear adjustment of an exponential function of the absorption [23,60]. SR was used as a proxy of the relative molecular weight and source of the DOM, with values < 1 indicative of enrichment in high-molecular-weight compounds, and higher values DOM consisting of lower molecular weight compounds [17,60].

2.7. Statistical Analyses

Comparisons of the mean values of studied parameters for the different stream corridor land covers (L) and hydrological months (H) for the two catchments were performed in SPSS 17.0 (SPSS Inc., Chicago, IL, USA) using univariate analysis of variance. When the requirements for parametric tests were not met, we used Tamhane's non-presumed equal-variance test. Data are presented as means \pm 95% confidence intervals to illustrate significant differences between means, which is appropriate because the Tamhane's test results were consistent with the degree of overlap between the confidence intervals. All graphics presented here were made using Sigmaplot version 12.5 (Systat Software Inc, San Jose, CA, USA).

The results were further explored using factor analysis on loadings from the principal component analysis to identify interdependencies between parameters (e.g., common factors) and to identify temporal and spatial clusters within the reduced parameter space. The factor analysis included T_w , pH, E_h , DOC concentrations and all DOM optical indexes (FI, HIX, BIX and SR) and fDOM components (C1, C2 and C3) identified from PARAFAC.

Results of all measurements are publicly available at the following link: <http://dx.doi.org/10.5683/SP2/OKJKR8>.

3. Results

3.1. Hydrograph, Precipitation, and Stream Discharge

The catchments showed different discharge profiles due to the variation in land cover (Figure 2). The hydrographs of the Dam catchment showed less variation over the months and had more baseflow during the driest periods of 2016 (May to November) (Table 1). Both basins were dominated by baseflow (87% for Forest and 80% for Dam) (Figure 2, Table 1). The largest stormflows occurred in November 2016 in the Dam catchment, which were not observed in the Forested catchment.

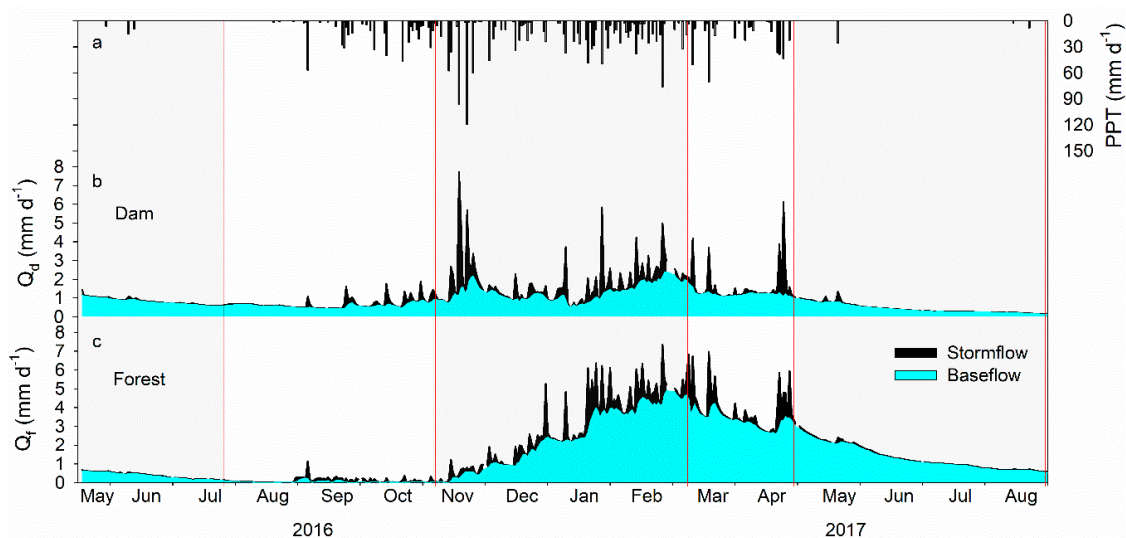


Figure 2. Daily variation of precipitation (a) and discharge in two headwater catchments (Q_d for the Dam (b), and Q_f for the Forest catchment (c)) at the research site. The graphs show data from May 2016 to August 2017 and the red vertical lines indicate sampling campaigns.

Despite the Dam catchment having the highest magnitude discharge during the study period, mean daily discharge was significantly ($p > 0.001$) greater in the Forest catchment (Figure 2, Table 1). The average daily discharge in the Forest catchment was 1.60 mm d^{-1} , and 1.04 mm d^{-1} in the Dam catchment with an accumulated discharge of 750.82 mm and 487.33 mm, respectively (Table 1). A significant relationship was found between accumulated precipitation and discharge only for the Dam catchment ($R^2 = 0.94$, $p = 0.006$) (Figure S3).

Table 1. Cumulative monthly precipitation (PPT) and discharge (Q_d for Dam and Q_f for Forest catchments), mean and median daily discharge, percent baseflow (BF) and stormflow (SF) with the discharge for hydrological months in pasture catchments at the research site.

Date	Month	PPT (mm)	Forest				Dam					
			Q_f (BF) (mm)	Q_f (mm d^{-1})		% BF	% SF	Q_d Accumulated (mm)	Q_d (mm d^{-1})		% BF	% SF
				Mean	Median				Mean	Median		
25/07/2016	Jul/16	32	26.9	0.38	0.40	94.9	5.1	59.0	0.84	0.81	96.6	3.4
05/11/2016	Nov/16	464	12.1	0.12	0.62	41.6	58.4	72.1	0.70	0.62	84.6	15.4
07/03/2017	Mar/17	1414	339.2	2.78	2.36	83.4	16.6	217.9	1.79	1.47	71.5	28.5
29/04/2017	Abr/17	403	205.5	3.88	3.55	86.5	13.5	83.5	1.57	1.25	77.4	22.6
28/08/2017	Aug/17	36	166.5	1.38	1.11	97.0	3.0	54.7	0.45	0.34	94.7	8.7
Total (study period)		2350	750.8					487.3				
Mean (study period)				1.60		87	13		1.04		80	20

3.2. Concentrations of DOC and Optical Characteristics of DOM

DOC concentrations in streams varied significantly between Dam and Forest catchments and between the hydrological months (Figure 3). DOC in the Forest catchment was $2.97 \pm 0.33 \text{ mg L}^{-1}$ (mean \pm CI), and $2.19 \pm 0.31 \text{ mg L}^{-1}$ in the Dam catchment. For both catchments, DOC was significantly greater during November 2016 in relation to the other hydrologic months following the onset of the rainy season (Figure 3 and Table S1). In the Forest catchment—in both the November 2016 and March 2017 months—the DOC values were significantly greater than in the Dam catchment (Figure 3) for the same period.

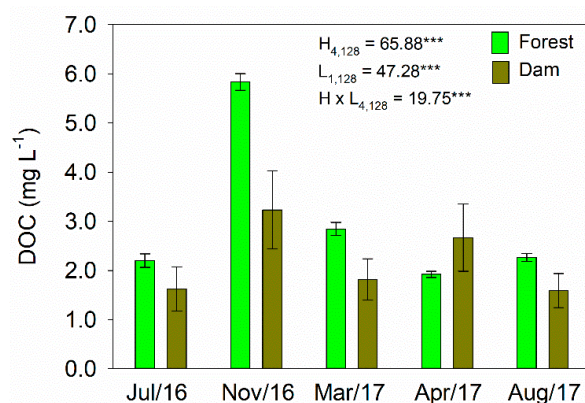


Figure 3. Mean dissolved organic carbon (DOC) ($\pm 95\%$ CI, $n = 11$ Dam; $n = 15$ Forest) at the research site, grouped by Dam and Forest catchments and hydrologic month. The statistical results are expressed using the Tamhane test of non-presumed equal variances and the probability of type I error (P) to test with land cover (L) and hydrological month (H) as fixed effects. *** $p < 0.001$.

Fluorescence index (FI) values varied between 1.29 and 1.41 during all months and for both catchments, indicating that DOC was predominantly derived from terrestrial sources in both areas ($FI < 1.5$) (Figure 4a, Table S1). The mean values of the FI showed significant differences between the catchments, with greater values in the Dam catchment in relation to the Forest catchment during all months (Figure 4a, Table S1). The values for spectral slope (SR) were significantly different between catchments and months for the complete set of data (Figure 4b). SR ranged from 0.74 to 1.25 and the highest SR values were found in the Dam catchment in all months compared to the Forest catchment (Figure 4b, Table S1). Higher variability among SR values for different sampling dates was found in the Dam catchment, mainly in months of July 2016, November 2016 and March 2017, which presented values suggesting DOM predominantly comprised of compounds with higher molecular weight (Figure 4b, Table S1).

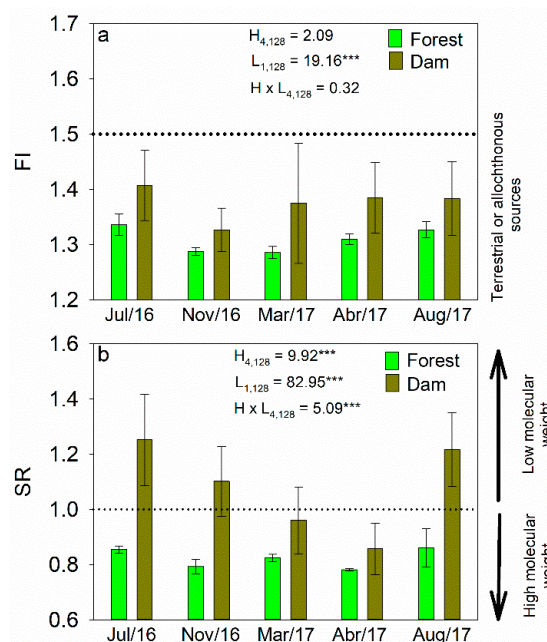


Figure 4. Mean ($\pm 95\%$ CI, $n = 11$ Dam; $n = 15$ Forest) at the research site, grouped by Dam and Forest catchments and hydrological month for (a) fluorescence index (FI) and (b) slope ratio (SR). The statistical results are expressed using the Tamhane test of non-presumed equal variances and the probability of type I error (P) to test with land cover (L) and hydrological month (H) as fixed effects. *** $p < 0.001$. Dotted lines indicate threshold values for FI [51] and SR [60].

The values of the humification index (HIX) showed a significant difference between catchments with different coverages and hydrological months (Figure 5a, Table S1). HIX values were always higher in the Forest catchment during all hydrological periods. HIX varied from 3.39 to 5.51, with an average value of 4.14 ± 0.21 reflecting more humic source material of mainly terrestrial origin. In contrast, the Dam catchment presented comparatively lower HIX values ranging from 1.37 to 2.93, with mean values around 2.15 ± 0.24 (Figure 5a, Table S1), with lower values indicative of autochthonous DOM that is more recently produced. Similar to HIX, the biological index (BIX) also presented a significant difference between catchments and between hydrological months (Figure 5b). BIX values were higher for the Dam catchment (0.95 ± 0.11) compared to Forest (0.69 ± 0.01) (Figure 5b, Table S1). During the month of July 2016, August 2017 and mainly March 2017, mean values of BIX were < 0.8 , corresponding to a more recent production of DOM of microbial origin (Figure 5b, Table S1).

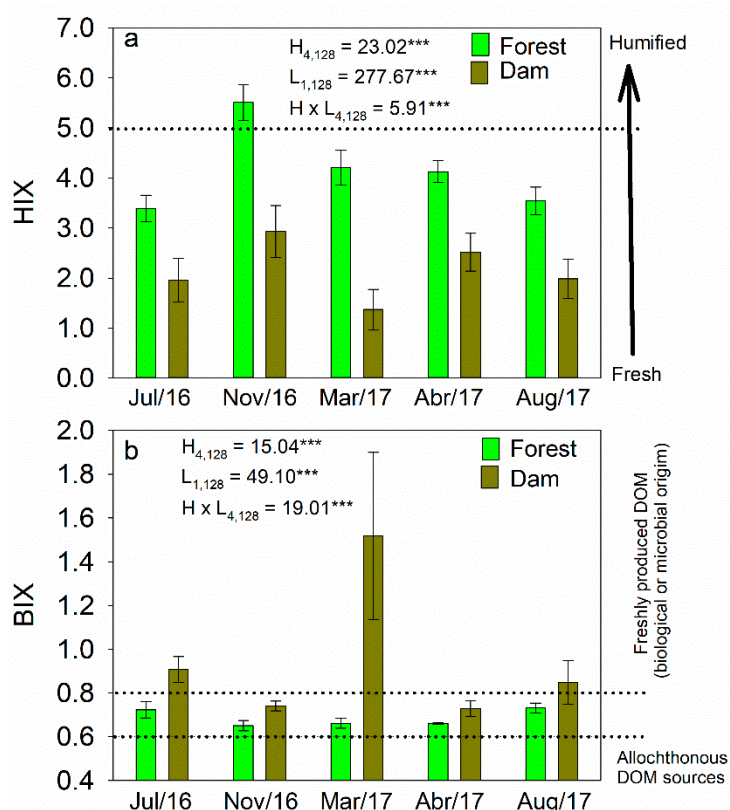


Figure 5. Mean ($\pm 95\%$ CI, $n = 11$ Dam; $n = 15$ Forest) at the research site, grouped by Dam and Forest catchments and hydrological month for (a) humification index (HIX) and (b) biological index (BIX). Statistical results are expressed using the Tamhane test of non-presumed equal variances and the probability of type I error (P) to test with land cover (L) and hydrological month (H) as fixed effects. $*** p < 0.001$. Dotted lines indicate threshold values for HIX and BIX for indicator values [58].

3.3. Fluorescence Characterization by PARAFAC

Based on the PARAFAC modeling of EEMs from water samples collected in both catchments, we validated a three component model (C1, C2, and C3) to characterize fDOM in the sample set (Table 2). These components were compared to the values of components described and archived in the OpenFluor database [48], indicating that C1 and C2 in the present study relate to terrestrial material comprised of humic-like fluorophores, whereas C3 was identified as having protein-like characteristics.

Table 2. Positions of excitation (Ex) emission (Em) maxima of the three components of fluorescent dissolved organic matter (fDOM) identified by the PARAFAC model using all collected samples independently collected in the Dam and Forest catchments. Two lines in the excitation (red lines) and emission (blue lines) spectra show half-split validation results.

Component 1			Component 2			Component 3		
Ex (nm)	Em (nm)	Contribution to total fDOM	Ex (nm)	Em (nm)	Contribution to total fDOM	Ex (nm)	Em (nm)	Contribution to total fDOM
<252 (357)	474	40.1%	<252 (321)	408	39.1%	288	333	20.8%
UV Humic-Like			Ubiquitous Humic-Like			Protein-Like		

Components C1 and C2 showed two excitation maxima in a single emission spectrum, as a combination of two fluorescent peaks (Table 2). Together, components C1 and C2 represented 79.22% of the DOM fluorophores. C1 had a primary excitation peak at < 252 nm and a secondary peak at 357 nm with a maximum emission peak at 474 nm, and C2 has a maximum primary excitation at < 252 nm a secondary peak at 321 nm showing an emission peak at 408 nm. Using the OpenFluor database [48], the C1 and C2 component were found to have a strong similarity (values > 0.95) for a variety of aquatic environments [15–17,20,27,61].

The C3 component had a maximum emission band at 333 nm for an excitation at 288 nm, with a fluorescent peak that resembles protein compounds [62] (Table 2). In addition, C3 represented 20.8% of the total fDOM in the complete set of data. A correspondence for C3 was identified in the OpenFluor database (similarity > 0.95) and resembled the spectral characteristics found in natural and anthropogenic systems [20,63,64].

The component percentages of total fDOM were significantly different between the catchments and hydrological months (Figure 6). The total fDOM in the two streams surveyed was almost entirely composed of terrestrially derived materials, as reflected by the aggregate percentages of components C1 and C2. The C1 component represented approximately 12% more of the fDOM signal in the Forest catchment, compared to the Dam catchment (Figure 6a,b, Table S1), whereas for C2 this difference between catchments was lower overall (~8%) and showed no significant difference in July 2016. In contrast to C1 and C2, component C3 was significantly greater in the Dam catchment (42.1 ± 1.3) compared to the Forest catchment (22.4 ± 4.0) (Figure 6c, Table S1). The total fDOM of C3 was significantly greater in all hydrologic months in the Dam catchment, especially in July 2016, August 2017 and mainly March 2017, when C3 represented ~60% of the total Dam fDOM.

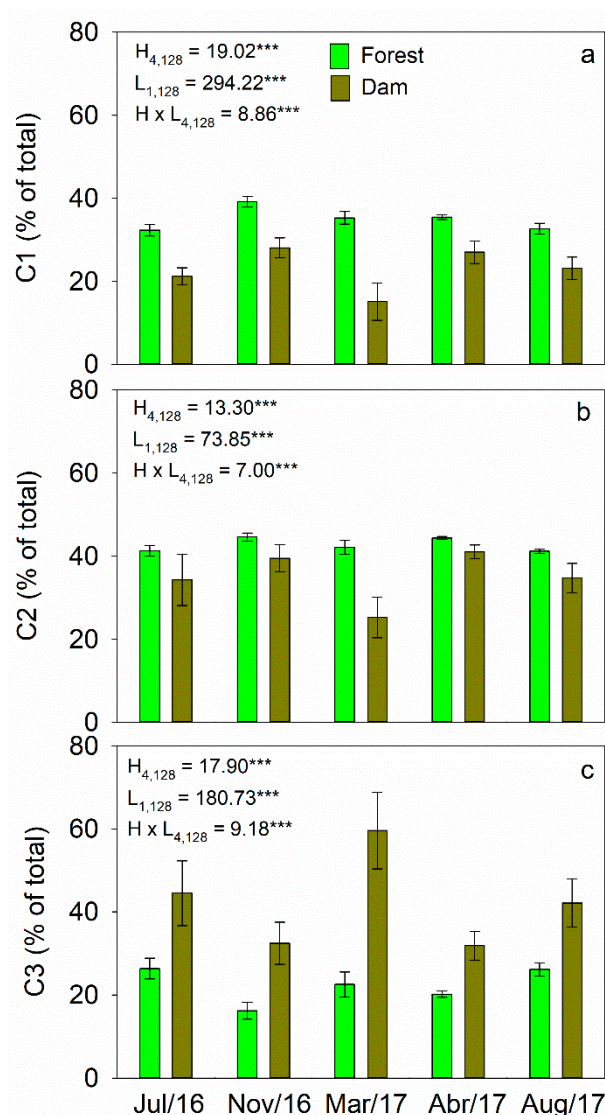


Figure 6. Mean (95% CI, $n = 11$ Dam; $n = 15$ Forest) at the research site, grouped by Dam and Forest catchments and hydrological month for percentages of the total fDOM for (a) C1, (b) C2, and (c) C3. The statistical results are expressed using the Tamhane test of non-presumed equal variances and the probability of type I error (P) to test with land cover (L) and hydrological month (H) as fixed effects. *** $p < 0.001$.

3.4. Principal Component Analysis (PCA)

Factor analysis was applied to all environmental variables (T_w , E_{hv} , pH, Table S2) and sample results including DOC concentrations, DOM optical indexes (SR, FI, HIX and BIX) and PARAFAC components C1, C2, and C3 (as % of total fDOM). This resulted in two main components explaining more than 62% of the total variance in the sample set (Figure 7). The first component (PC1) showed a transition from a more aromatic terrestrial DOM (HIX (0.81), C1 (0.91), positive charges) with a higher presence in the Forest catchment for a DOM of more protein origin (C3 (-0.93), BIX (-0.85), negative load) found mainly in for the Dam catchment. The most significant factors for PC2 were DOC (0.88) and T_w (0.58). The variations between hydrological periods were consistent with the understanding that the humic type DOM is transported from the terrestrial environment with greater vegetation cover to the hydrosphere during months of high precipitation, thereby mobilizing terrestrial C to the hydrosphere in November 2016 following the dry season.

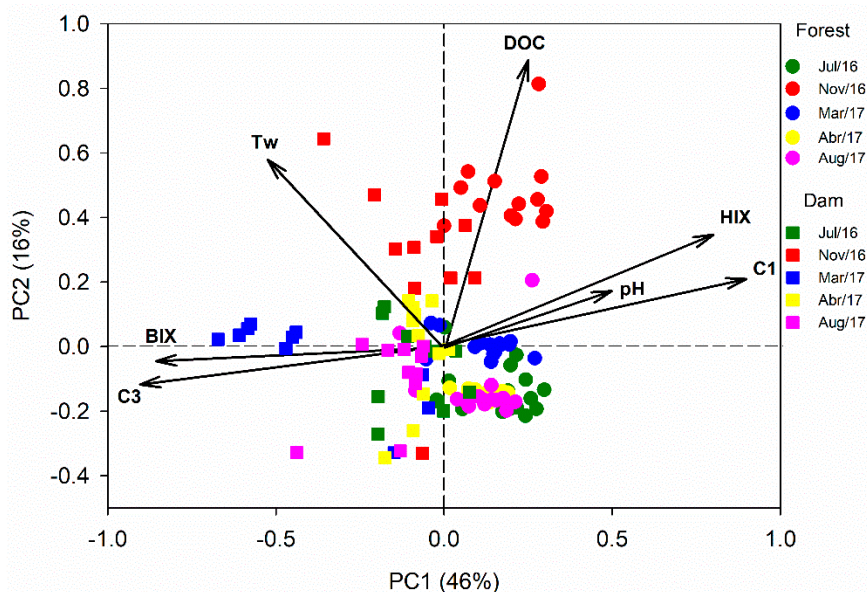


Figure 7. Graphical representation of the load factors for the input variables and scores plot for water samples collected in the different catchments (square for Dam and circle for Forest) and hydrological month (different colors).

4. Discussion

4.1. Variations of Hydrology in Dam and Forest Catchments

Recent studies in Amazonia have shown that land cover strongly affects stream discharge [5,10,65]. We found a 1.5 fold reduction in discharge for the pasture catchment with the dammed stream compared to the pasture catchment with a riparian forest buffer. This difference may be related to increased evaporation, infiltration, and water consumption for livestock. Soil porewater proximal to the ground (approximately 2 m) is available for plants, leaving a larger volume of water to move and be exported from catchments [66]. Evaporation losses represent about 5% of total global river flows [67,68], and depending on the livestock density (as cattle per unit area), water consumption may be significant. For instance, cattle weighing between 250–455 kg can drink approximately 42 L of water per day [69,70].

Discharge in the Dam catchment showed a greater response to precipitation compared to the Forest catchment (Figure S3). This relationship may be associated with soil compaction in pastures where there is no riparian forest (where livestock has access to the stream banks [71]), which we also relate to stormflow (20% of the total flow of the catchment) during the major rainfall events, thus reinforcing this connectivity between precipitation and discharge (Table 1). The greater stream slope in the Dam catchment (0.031 m m^{-1}) could be a secondary factor in the higher runoff ratio for the Dam catchment compared to the Forest catchment.

The lack of significant relationship in the Forest catchment ($R^2 = 0.53$, $p = 0.163$) was likely due to a more buffered hydrological system (Figure S3, Table 1) coupled with a lower stream slope (0.011 m m^{-1}) (Figure 1), showing a possible response to delayed precipitation inputs. In the July 2016 hydrological month, accumulated precipitation was 32 mm and mean discharge was 0.38 mm d^{-1} , while in November 2016 the lowest discharge (0.12 mm d^{-1}) was observed for the largest precipitation (466 mm). This lagged response between onset of the rainy season and corresponding rise in streamflow has been reported for other forested watersheds in the region [9]. Germer et al. [72] studied the influence of land use change on hydrological processes for undisturbed forested and grazing areas in the Amazon basin and found a 17-fold increase in stormflow in pasture areas due to soil compaction and an increase in hydraulic conductivity. On the other hand, Neill et al. [73] found that land cultivated with soybeans showed little difference in soil infiltration and saturated soil

hydraulic conductivity compared to native forests. They concluded that current cropping practices such as no-till agriculture avoid generating horizontal water flows, surficial gullying, and erosion that occur commonly in Amazon pastures [72].

Baseflow in the Forest catchment was slightly below other forested catchments measured in Southern Amazonia (94 and 98 % of streamflow) [10,74]. This difference is likely due to the mosaic land cover of the Forest catchment which was comprised of pasture cover for areas more distant from the stream, and riparian forest cover for areas closer to the stream. The higher baseflow in the Forest catchment compared to the Dam catchment may be related to rapid recharge rates due to macropores, as opposed to groundwater recharge in the Pasture catchment which may be slower, suggesting a potential alteration of fundamental mechanisms in headwater streamflow generation [72]. Our results suggest that a forest to pasture conversion with dammed streams could increase the stormflow component of stream discharge, which may occur via alterations in hydrologic flowpaths (i.e., the way in which water travels through soil and groundwater and/or over the soil surface towards the main channel).

4.2. Seasonal Variability in DOC and Optical Properties of DOM

In addition to land cover effects on stream discharge, seasonal precipitation was found to strongly influence stream water quality as evidenced by seasonal variability found for DOC concentration and DOM characteristics. DOC concentration was greater during the first large precipitation events following the dry season and gradually decreased as the rainy season progressed, indicating a dilution of C flowing from the ecosystem landscape, though this effect was lagged in the Forest catchment. This conclusion is in agreement with observations of Xu and Saiers [75] who showed that the amount of DOM mobilized by water infiltration varies with the intensity and frequency of rainfall. In addition, the increase in DOC concentration during November 2016 may also be related to the accumulation of organic C in the forest canopy, litter layer and near-surface soil horizons during dry periods which was subsequently moved to streams during precipitation events [2,74].

DOM optical characteristics during all hydrological months were more aromatic for the Forest catchment as indicated by FI values. These characteristics are generally derived from terrestrial soils and vascular plant sources [26,76]. In contrast, the Dam catchment exhibited a gradual reduction in FI from July 2016 to November 2017, and the SR values indicating DOM with low molecular weight during the dry season (July 2016) and early rainy season (November 2016) compared with SR values indicating high molecular weight DOM for March 2017 and April 2017 (Figure 4). These changes illustrate the role of hydrological connectivity in the transport of DOM to water bodies. During the periods of lower flow/precipitation, the water bodies in the pasture with dams and without riparian forest tend to have a longer residence time and a higher incidence of solar radiation favoring DOC losses through photochemical degradation and/or microbial processes and photodegradation, thus leading to a low molecular weight and DOM aromaticity. On the other hand, the period of higher accumulated precipitation, the DOM exhibited stronger aromatic characteristics, with low SR values and low and relatively constant FI values, indicating a greater mobilization of fresh DOM with high molecular weights and more aromatic compounds [27,76]. In the Forest catchments, SR values throughout the study period indicated a predominance of higher molecular weight compounds (lower values of SR) with greater aromaticity mainly derived from leachate vascular plant inputs from the forest.

The HIX values for the Forest catchment showed reductions over the November 2016 to August 2017 period. This pattern is consistent with the role of forest landscapes in the transfer of DOM to tropical freshwater systems, in which DOM derived from tropical forests is more aromatic than DOM from other land cover types [77], which can be transported during periods of higher rainfall, thereby increasing the organic compounds dissolved in the soil litter layer and from near-surface soil organic matter. According to Williams et al. [20] HIX values increase with DOC concentration in areas

with a higher proportion of riparian forest, but HIX was not found to correlate with agricultural and human uses.

BIX values > 0.8 correspond to DOM of microbial origin, whereas values < 0.6 are considered to contain little autochthonous DOM [58]. The BIX values for the Forest catchment studied varied between 0.6 and 0.8 corresponding to a mixture of primarily allochthonous DOM with minor contribution of autochthonous DOM [58] during all studied hydrological periods. The Dam catchments exhibited BIX values > 1.0 during July 2016, August 2017 and particularly March 2017, corresponding to a predominantly autochthonous (microbial) DOM and the presence of freshly released DOM in the water. These results support the hypothesis of Wilson and Xenopoulos [78] that high BIX ratios represent microbially produced recently produced DOM.

The contribution of components C1 and C2 to total fluorescence did not vary much over the study period in the Forest catchment, while the Dam catchment showed large variations in fluorescence signature (Figure 6a,b). Despite the little variation for the Forest catchment, C1 during November 2016 differed significantly from the other months, and was associated with higher HIX during that month. This increase in HIX early in the rainy season suggests an allochthonous source linked to runoff or leachate from the soil [27]. Thus, it seems that C1 acts as an indicator of allochthonous inputs from soil and the litter layer [76]. Component C3 was present in greater proportions in the Dam catchment during the wetter month (March 2017; Figure 6c). This was also related to the lower HIX and higher BIX values observed. This increase of C3 can occur due to free amino acids that are released when organic matter is decomposed by increasing relative autochthonous DOM contributions during hot and humid conditions [28,44,76]. Similar patterns were observed Yamashita et al. [27] in first- to third-order streams, suggesting that high levels of protein-like components during the growing season may be related to recent biological activity and that these components are part of the semi-labile fraction.

4.3. Effects of Land Cover on Optical Properties of DOM in Headwater Catchments

We found that the concentration of DOC and DOM characterization in the dammed stream and the stream with a riparian buffer were significantly influenced by stream corridor land cover. Such differences may be due to changes in hydrological flowpath activation affecting inputs of organic matter to the riverine zone, and differences in within-stream biological activity [79]. The presence of livestock in catchments acted to increase DOM processing rates compared to those observed in streams with forest vegetation [20]. The optical character of the DOM in the Dam catchment were structurally less complex. Studies in the Coweeta watersheds have reported that the relative contributions of protein-like components are greater in managed/disturbed river basins compared to forested ones [27]. In the present study, DOM in the Dam catchment tended to show smaller molecular weights SR and lower HIX values than DOM in the Forest catchment, which presented higher humification and more complex compounds.

The protein-like component (C3) was present in both headwater catchments, with an overall relative abundance of 22% of the total fDOM for the Forest catchment and 42% of total fDOM for the Dam catchment. Significantly greater values for C3 and BIX in the Dam catchment indicate more microbially derived DOM. It is believed that protein-like fluorophores are produced and consumed by microorganisms [80,81] and tend to increase in areas influenced by anthropogenic activities [20,21,82,83]. In livestock grazing areas in Southern Amazonia, impoundments are established in pastures as a source of drinking water [10]. Changes in the optical properties of DOM in the Dam stream may be due to the increase in primary productivity (microbial activity) caused by the longer residence time of the water in the impoundments that favor the physical-chemical and biological degradation of the leachate [21], along with the increase in stream temperature from radiation, thereby increasing the production of degradation materials that fluoresce both protein and phenolic materials [17,84]. In addition, radiation can reduce the molecular weight of DOMs by direct photodegradation and by stimulating autochthonous production of protein-like components [85].

Approximately 78% of the total DOM fluorescence in the Forest catchment and 58% in the Dam catchment included components similar to humic material (C1 and C2) derived from terrestrial plants or organic matter of the soil [86] with an aromatic chemical nature, higher molecular weight and high HIX values that are indicative of highly-humified DOM [52,54] are common in soils with native vegetation [18]. The fraction of humic-like fDOM in Dam catchment was 42% overall. The C1 and C2 components were much more abundant in the catchment with the forest buffer, and were likely derived from older soil organic matter [27]. Soils in areas with forest cover receive years of leaf litter that decompose rapidly, thereby increasing to DOC entries to soil water and streams [2].

5. Conclusion

Statistical analyses showed that differences in land cover and related differences in hydrologic processes (stormflow versus baseflow) were responsible for variations in DOC concentrations and optical properties of DOM. DOM in the stream with a riparian forest buffer was mainly derived from soil and plant material, although recent organic production DOC (protein-like) also is evident. The pasture catchment containing the dams exhibited a predominance of DOM with a microbially-derived character, largely due to damming and the absence of riparian forest, which contributed to altering the hydrological, thermal and transmissive connectivity of the hydrologic system. The results of this study suggest that changes in land cover of stream corridors can result in altered hydrology and C cycling. Given that these land cover changes persist over multiple decades, these anthropogenically induced transformations in the region may have significant implications for downstream water quality in the Amazon basin.

Supplementary Materials: The following are available online at <http://www.mdpi.com/2073-4441/11/2/390/s1>, Table S1: Mean ($\pm 95\%$ CI, $n = 11$ Dam; $n = 15$ Forest), minimum and maximum pH, oxidation-reduction potential (E_h) and water temperature (T_w) by month for Dam and Forest catchments at the research site. Table S2: Mean ($\pm 95\%$ CI), minimum and maximum dissolved organic carbon (DOC), fluorescence index (FI), spectral slope ratio (SR), humification index (HIX), biological index (BIX), and relative abundance of each PARAFAC component (% of total fDOM) by month in the Dam and Forest catchments at the research site. Figure S1: Power functions between discharge and water level (WL) in Forest and Dam catchments at Pedra Alta Ranch near Alta Floresta, Mato Grosso, Brazil. Figure S2: Calibration curve for DOC concentrations developed using IHSS SRHA standard II (2S10H). Figure S3: Linear regressions of Forest (a) and Dam (b) catchment cumulative discharge (Q , mm) versus cumulative precipitation (PPT, mm) in the hydrological months.

Author Contributions: Conceptualization, M.J.L. and M.S.J.; Methodology, M.S.J.; Formal Analysis, F.d.S.S. and O.B.P.; Investigation, H.J.D. and M.F.G.; Resources, E.G.C.; Data Curation, P.H.Z.d.A.; Writing—Original Draft Preparation, H.J.D. and M.S.J.; Writing—Review and Editing, H.J.D., M.S.J., and M.J.L.; Visualization, H.J.D.; Supervision, M.S.J.; Project Administration, H.J.D.; Funding Acquisition, H.J.D.

Funding: This work constitutes a contribution to the project entitled “*Avaliação da qualidade do carbono orgânico dissolvido em riachos com diferentes usos do solo na região sul da Amazônia*” funded by the Foundation for Research Support of the State of Mato Grosso (FAPEMAT) (221934/2015 to H.J.D.). This study also contributes to the project “*Carbon and ecohydrology of Mato Grosso ecosystems and agroecosystems*” funded by the Coordination of Improvement of Higher Education Personnel (CAPES) science mobilization program Science without Borders (2366/2012 to E.G.C. and M.S.J.).

Acknowledgments: We thank Mr. Clóvis Siqueira de Brito, owner of Pedra Alta ranch for making the study area available. We are very grateful for the laboratory space and logistic support provided by Francisco de Almeida Lobo, Carmen Eugenia Rodríguez Ortíz, Ricardo Santos Amorim and Suzana Souza dos Santos from the Federal University of Mato Grosso (UFMT), and to all employees of Pedra Alta ranch.

Conflicts of Interest: The authors declare no conflict of interest.

References

1. Malhi, Y.; Roberts, J.; Betts, R.; Killeen, T.; Li, W.; Nobre, C. Climate change, deforestation, and the fate of the amazon. *Science* **2008**, *319*, 169–172. [[CrossRef](#)] [[PubMed](#)]
2. Neu, V.; Ward, N.D.; Krusche, A.V.; Neill, C. Dissolved organic and inorganic carbon flow paths in an Amazonian transitional forest. *Front. Mar. Sci.* **2016**, *3*, 114. [[CrossRef](#)]

3. Lathuillière, M.J.; Coe, M.T.; Johnson, M.S. A review of green- and blue-water resources and their trade-offs for future agricultural production in the Amazon basin: What could irrigated agriculture mean for Amazonia? *Hydrol. Earth Syst. Sci.* **2016**, *20*, 2179–2194. [[CrossRef](#)]
4. Food and Agriculture Organization of the United Nations. *Global Forest Resources Assessment 2015*, 2nd ed.; FAO: Rome, Italy, 2015.
5. Levy, M.; Lopes, A.; Cohn, A.; Larsen, L.; Thompson, S. Land use change increases streamflow across the arc of deforestation in Brazil. *Geophys. Res. Lett.* **2018**, *45*, 3520–3530. [[CrossRef](#)]
6. INPE. Projeto Prodes, Monitoramento da Floresta Amazonica Brasileira por Satelite. Available online: <http://www.obt.inpe.br/prodes/dashboard/prodes-rates.html> (accessed on 14 October 2018).
7. Macedo, M.N.; DeFries, R.S.; Morton, D.C.; Stickler, C.M.; Galford, G.L.; Shimabukuro, Y.E. Decoupling of deforestation and soy production in the southern Amazon during the late 2000s. *Proc. Natl. Acad. Sci. USA* **2012**, *109*, 1341–1346. [[CrossRef](#)] [[PubMed](#)]
8. Barona, E.; Ramankutty, N.; Hyman, G.; Coomes, O.T. The role of pasture and soybean in deforestation of the Brazilian Amazon. *Environ. Res. Lett.* **2010**, *5*, 024002. [[CrossRef](#)]
9. Johnson, M.S.; Lehmann, J.; Riha, S.J.; Krusche, A.V.; Richey, J.E.; Ometto, J.P.H.; Couto, E.G. CO₂ efflux from Amazonian headwater streams represents a significant fate for deep soil respiration. *Geophys. Res. Lett.* **2008**, *35*. [[CrossRef](#)]
10. Hayhoe, S.J.; Neill, C.; Porder, S.; McHorney, R.; Lefebvre, P.; Coe, M.T.; Elsenbeer, H.; Krusche, A.V. Conversion to soy on the Amazonian agricultural frontier increases streamflow without affecting stormflow dynamics. *Glob. Chang. Biol.* **2011**, *17*, 1821–1833. [[CrossRef](#)]
11. Macedo, M.N.; Coe, M.T.; DeFries, R.; Uriarte, M.; Brando, P.M.; Neill, C.; Walker, W.S. Land-use-driven stream warming in southeastern Amazonia. *Phil. Trans. R. Soc. B* **2013**, *368*, 20120153. [[CrossRef](#)] [[PubMed](#)]
12. Ågren, A.; Berggren, M.; Laudon, H.; Jansson, M. Terrestrial export of highly bioavailable carbon from small boreal catchments in spring floods. *Freshw. Biol.* **2008**, *53*, 964–972. [[CrossRef](#)]
13. Laudon, H.; Berggren, M.; Ågren, A.; Buffam, I.; Bishop, K.; Grabs, T.; Jansson, M.; Köhler, S. Patterns and dynamics of dissolved organic carbon (DOC) in boreal streams: The role of processes, connectivity, and scaling. *Ecosystems* **2011**, *14*, 880–893. [[CrossRef](#)]
14. McElmurry, S.P.; Long, D.T.; Voice, T.C. Stormwater dissolved organic matter: Influence of land cover and environmental factors. *Environ. Sci. Technol.* **2013**, *48*, 45–53. [[CrossRef](#)] [[PubMed](#)]
15. Garcia, R.D.; Reissig, M.; Queimaliños, C.P.; Garcia, P.E.; Dieguez, M.C. Climate-driven terrestrial inputs in ultraligotrophic mountain streams of Andean Patagonia revealed through chromophoric and fluorescent dissolved organic matter. *Sci. Total Environ.* **2015**, *521*, 280–292. [[CrossRef](#)] [[PubMed](#)]
16. Dalmagro, H.J.; Johnson, M.S.; Musis, C.R.; Lathuillière, M.J.; Graesser, J.; Junior, O.B.; Couto, E.G. Spatial patterns of DOC concentration and DOM optical properties in a Brazilian tropical river-wetland system. *J. Geophys. Res. Biogeosci.* **2017**, *122*, 1883–1902. [[CrossRef](#)]
17. Lambert, T.; Teodoru, C.R.; Nyoni, F.C.; Borges, A.V. Along-stream transport and transformation of dissolved organic matter in a large tropical river. *Biogeosciences* **2016**, *13*, 2727–2741. [[CrossRef](#)]
18. Wilson, H.F.; Xenopoulos, M.A. Ecosystem and seasonal control of stream dissolved organic carbon along a gradient of land use. *Ecosystems* **2008**, *11*, 555–568. [[CrossRef](#)]
19. Yamashita, Y.; Scinto, L.J.; Maie, N.; Jaffé, R. Dissolved organic matter characteristics across a subtropical wetland's landscape: Application of optical properties in the assessment of environmental dynamics. *Ecosystems* **2010**, *13*, 1006–1019. [[CrossRef](#)]
20. Williams, C.J.; Yamashita, Y.; Wilson, H.F.; Jaffé, R.; Xenopoulos, M.A. Unraveling the role of land use and microbial activity in shaping dissolved organic matter characteristics in stream ecosystems. *Limnol. Oceanogr.* **2010**, *55*, 1159–1171. [[CrossRef](#)]
21. Jaffé, R.; McKnight, D.; Maie, N.; Cory, R.; McDowell, W.; Campbell, J. Spatial and temporal variations in DOM composition in ecosystems: The importance of long-term monitoring of optical properties. *J. Geophys. Res. Biogeosci.* **2008**, *113*. [[CrossRef](#)]
22. Fellman, J.B.; Hood, E.; Edwards, R.T.; D'Amore, D.V. Changes in the concentration, biodegradability, and fluorescent properties of dissolved organic matter during stormflows in coastal temperate watersheds. *J. Geophys. Res. Biogeosci.* **2009**, *114*. [[CrossRef](#)]

23. Spencer, R.G.; Stubbins, A.; Hernes, P.J.; Baker, A.; Mopper, K.; Aufdenkampe, A.K.; Dyda, R.Y.; Mwamba, V.L.; Mangangu, A.M.; Wabakanghanzi, J.N. Photochemical degradation of dissolved organic matter and dissolved lignin phenols from the Congo River. *J. Geophys. Res. Biogeosci.* **2009**, *114*. [[CrossRef](#)]
24. Singh, S.; Inamdar, S.; Scott, D. Comparison of two parafac models of dissolved organic matter fluorescence for a mid-atlantic forested watershed in the USA. *J. Ecosyst.* **2013**, *2013*, 532424. [[CrossRef](#)]
25. Mariot, M.; Dudal, Y.; Furian, S.; Sakamoto, A.; Vallès, V.; Fort, M.; Barbiero, L. Dissolved organic matter fluorescence as a water-flow tracer in the tropical wetland of Pantanal of Nhecolândia, Brazil. *Sci. Total Environ.* **2007**, *388*, 184–193. [[CrossRef](#)] [[PubMed](#)]
26. Fellman, J.B.; Hood, E.; Spencer, R.G. Fluorescence spectroscopy opens new windows into dissolved organic matter dynamics in freshwater ecosystems: A review. *Limnol. Oceanogr.* **2010**, *55*, 2452–2462. [[CrossRef](#)]
27. Yamashita, Y.; Kloeppel, B.D.; Knoepp, J.; Zausen, G.L.; Jaffé, R. Effects of watershed history on dissolved organic matter characteristics in headwater streams. *Ecosystems* **2011**, *14*, 1110–1122. [[CrossRef](#)]
28. Stedmon, C.A.; Markager, S.; Bro, R. Tracing dissolved organic matter in aquatic environments using a new approach to fluorescence spectroscopy. *Mar. Chem.* **2003**, *82*, 239–254. [[CrossRef](#)]
29. Larsen, L.G.; Aiken, G.R.; Harvey, J.W.; Noe, G.B.; Crimaldi, J.P. Using fluorescence spectroscopy to trace seasonal DOM dynamics, disturbance effects, and hydrologic transport in the Florida Everglades. *J. Geophys. Res. Biogeosci.* **2010**, *115*. [[CrossRef](#)]
30. Fasching, C.; Behounek, B.; Singer, G.A.; Battin, T.J. Microbial degradation of terrigenous dissolved organic matter and potential consequences for carbon cycling in brown-water streams. *Sci. Rep.* **2014**, *4*, 4981. [[CrossRef](#)] [[PubMed](#)]
31. Baker, A. Fluorescence properties of some farm wastes: Implications for water quality monitoring. *Water Res.* **2002**, *36*, 189–195. [[CrossRef](#)]
32. Dubreuil, V.; Debortoli, N.; Funatsu, B.; Nédélec, V.; Durieux, L. Impact of land-cover change in the southern Amazonia climate: A case study for the region of Alta Floresta, Mato Grosso, Brazil. *Environ. Monit. Assess.* **2012**, *184*, 877–891. [[CrossRef](#)] [[PubMed](#)]
33. International Union of Soil Sciences Working Group WRB. *World Reference Base for Soil Resources 2014 (Update 2015), International Soil Classification System for Naming Soils and Creating Legends for Soil Maps*; World Soil Resources Report No. 106; FAO: Rome, Italy, 2015.
34. Santos, V. Análise florística e Estrutural de uma Floresta Ombrófila Aberta Primária no Parque Estadual Cristalino, Alta Floresta–MT. Master’s Dissertation, Universidade Estadual do Mato Grosso, Alta Floresta, Brazil, 2005.
35. Hund, S.V.; Johnson, M.S.; Keddie, T. Developing a hydrologic monitoring network in data-scarce regions using open-source Arduino dataloggers. *Agric. Environ. Lett.* **2016**, *1*. [[CrossRef](#)]
36. Cunha, S.B.D.; Guerra, A.J.T. *Geomorfologia: Exercícios, Técnicas e Aplicações*; Bertand Brazil: Rio de Janeiro, Brazil, 1996; p. 345, ISBN 8528605485.
37. Ladson, A.; Brown, R.; Neal, B.; Nathan, R. A standard approach to baseflow separation using the Lyne and Hollick filter. *Australas. J. Water Resour.* **2013**, *17*, 25–34. [[CrossRef](#)]
38. Lyne, V.; Hollick, M. Stochastic Time-Variable Rainfall-Runoff Modelling. In Proceedings of the Institute of Engineers Australia National Conference: Engineering Management—update, Melbourne, Australia, 21–22 March 1979; pp. 89–93.
39. Dalmagro, H.J.; Lathuillière, M.J.; Hawthorne, I.; de Moraes, D.; Pinto Júnior, O.B.; Couto, E.G.; Johnson, M.S. Carbon biogeochemistry of a flooded Pantanal forest over three annual flood cycles. *Biogeochemistry* **2018**, *139*, 1–18. [[CrossRef](#)]
40. Vepraskas, M.J.; Faulkner, S. Redox chemistry of hydric soils. In *Wetland Soils: Genesis, Hydrology, Landscapes, and Classification*; Vepraskas, M.J., Richardson, J.L., Vepraskas, M.J., Craft, C.B., Eds.; CRC Press: Boca Raton, MA, USA, 2000; p. 432.
41. Dalmagro, H.J.; Lathuillière, M.J.; Vourlitis, G.L.; Campos, R.C.; Pinto, O.B.; Johnson, M.S.; Ortíz, C.E.; Lobo, F.D.A.; Couto, E.G. Physiological responses to extreme hydrological events in the Pantanal wetland: Heterogeneity of a plant community containing super-dominant species. *J. Veg. Sci.* **2016**, *27*, 568–577. [[CrossRef](#)]
42. Eykelbosh, A.J.; Johnson, M.S.; Couto, E.G. Biochar decreases dissolved organic carbon but not nitrate leaching in relation to vinasse application in a Brazilian sugarcane soil. *J. Environ. Manag.* **2015**, *149*, 9–16. [[CrossRef](#)] [[PubMed](#)]

43. Murphy, K.R.; Stedmon, C.A.; Graeber, D.; Bro, R. Fluorescence spectroscopy and multi-way techniques. PARAFAC. *Anal. Methods* **2013**, *5*, 6557–6566. [[CrossRef](#)]
44. Stedmon, C.A.; Markager, S. Resolving the variability in dissolved organic matter fluorescence in a temperate estuary and its catchment using PARAFAC analysis. *Limnol. Oceanogr.* **2005**, *50*, 686–697. [[CrossRef](#)]
45. Massicotte, M.P. Package ‘eemr’. 2016. Available online: <http://cran.fhcr.org/web/packages/eemR/eemR.pdf> (accessed on 10 May 2018).
46. Lawaetz, A.J.; Stedmon, C.A. Fluorescence intensity calibration using the Raman scatter peak of water. *Appl. Spectrosc.* **2009**, *63*, 936–940. [[CrossRef](#)] [[PubMed](#)]
47. Stedmon, C.A.; Bro, R. Characterizing dissolved organic matter fluorescence with parallel factor analysis: A tutorial. *Limnol. Oceanogr. Methods* **2008**, *6*, 572–579. [[CrossRef](#)]
48. Murphy, K.R.; Stedmon, C.A.; Wenig, P.; Bro, R. Openfluor—An online spectral library of auto-fluorescence by organic compounds in the environment. *Anal. Methods* **2014**, *6*, 658–661. [[CrossRef](#)]
49. Wang, Y.; Zhang, D.; Shen, Z.; Chen, J.; Feng, C. Characterization and spacial distribution variability of chromophoric dissolved organic matter (CDOM) in the Yangtze estuary. *Chemosphere* **2014**, *95*, 353–362. [[CrossRef](#)] [[PubMed](#)]
50. Cory, R.M.; McKnight, D.M. Fluorescence spectroscopy reveals ubiquitous presence of oxidized and reduced quinones in dissolved organic matter. *Environ. Sci. Technol.* **2005**, *39*, 8142–8149. [[CrossRef](#)] [[PubMed](#)]
51. McKnight, D.M.; Boyer, E.W.; Westerhoff, P.K.; Doran, P.T.; Kulbe, T.; Andersen, D.T. Spectrofluorometric characterization of dissolved organic matter for indication of precursor organic material and aromaticity. *Limnol. Oceanogr.* **2001**, *46*, 38–48. [[CrossRef](#)]
52. Huguët, A.; Vacher, L.; Relexans, S.; Saubusse, S.; Froidefond, J.-M.; Parlanti, E. Properties of fluorescent dissolved organic matter in the Gironde Estuary. *Org. Geochem.* **2009**, *40*, 706–719. [[CrossRef](#)]
53. Zsolnay, A.; Baigar, E.; Jimenez, M.; Steinweg, B.; Saccomandi, F. Differentiating with fluorescence spectroscopy the sources of dissolved organic matter in soils subjected to drying. *Chemosphere* **1999**, *38*, 45–50. [[CrossRef](#)]
54. Ohno, T. Fluorescence inner-filtering correction for determining the humification index of dissolved organic matter. *Environ. Sci. Technol.* **2002**, *36*, 742–746. [[CrossRef](#)] [[PubMed](#)]
55. Ohno, T.; Bro, R. Dissolved organic matter characterization using multiway spectral decomposition of fluorescence landscapes. *Soil Sci. Soc. Am. J.* **2006**, *70*, 2028–2037. [[CrossRef](#)]
56. Ohno, T.; Chorover, J.; Omoike, A.; Hunt, J. Molecular weight and humification index as predictors of adsorption for plant-and manure-derived dissolved organic matter to goethite. *Eur. J. Soil Sci.* **2007**, *58*, 125–132. [[CrossRef](#)]
57. Hunt, J.F.; Ohno, T. Characterization of fresh and decomposed dissolved organic matter using excitation–emission matrix fluorescence spectroscopy and multiway analysis. *J. Agric. Food Chem.* **2007**, *55*, 2121–2128. [[CrossRef](#)] [[PubMed](#)]
58. Birdwell, J.E.; Engel, A.S. Characterization of dissolved organic matter in cave and spring waters using UV–vis absorbance and fluorescence spectroscopy. *Org. Geochem.* **2010**, *41*, 270–280. [[CrossRef](#)]
59. Yamashita, Y.; Fichot, C.G.; Shen, Y.; Jaffé, R.; Benner, R. Linkages among fluorescent dissolved organic matter, dissolved amino acids and lignin-derived phenols in a river-influenced ocean margin. *Front. Mar. Sci.* **2015**, *2*, 92. [[CrossRef](#)]
60. Helms, J.R.; Stubbins, A.; Ritchie, J.D.; Minor, E.C.; Kieber, D.J.; Mopper, K. Absorption spectral slopes and slope ratios as indicators of molecular weight, source, and photobleaching of chromophoric dissolved organic matter. *Limnol. Oceanogr.* **2008**, *53*, 955–969. [[CrossRef](#)]
61. Graeber, D.; Gelbrecht, J.; Pusch, M.T.; Anlanger, C.; von Schiller, D. Agriculture has changed the amount and composition of dissolved organic matter in central European headwater streams. *Sci. Total Environ.* **2012**, *438*, 435–446. [[CrossRef](#)] [[PubMed](#)]
62. Coble, P.G. Marine optical biogeochemistry: The chemistry of ocean color. *Chem. Rev.* **2007**, *107*, 402–418. [[CrossRef](#)] [[PubMed](#)]
63. Osburn, C.L.; Wigdahl, C.R.; Fritz, S.C.; Saros, J.E. Dissolved organic matter composition and photoreactivity in prairie lakes of the US Great Plains. *Limnol. Oceanogr.* **2011**, *56*, 2371–2390. [[CrossRef](#)]
64. Baker, A. Fluorescence excitation–emission matrix characterization of some sewage-impacted rivers. *Environ. Sci. Technol.* **2001**, *35*, 948–953. [[CrossRef](#)] [[PubMed](#)]

65. Coe, M.; Latrubesse, E.; Ferreira, M.; Amsler, M. The effects of deforestation and climate variability on the streamflow of the Araguaia River, Brazil. *Biogeochemistry* **2011**, *105*, 119–131. [[CrossRef](#)]
66. von Randow, C.; Manzi, A.O.; Kruijt, B.; De Oliveira, P.; Zanchi, F.; Silva, R.; Hodnett, M.; Gash, J.; Elbers, J.; Waterloo, M. Comparative measurements and seasonal variations in energy and carbon exchange over forest and pasture in South West Amazonia. *Theor. Appl. Climatol.* **2004**, *78*, 5–26. [[CrossRef](#)]
67. Lehner, B.; Liermann, C.R.; Revenga, C.; Vörösmarty, C.; Fekete, B.; Crouzet, P.; Döll, P.; Endejan, M.; Frenken, K.; Magome, J. High-resolution mapping of the world's reservoirs and dams for sustainable river-flow management. *Front. Ecol. Environ.* **2011**, *9*, 494–502. [[CrossRef](#)]
68. Shiklomanov, I.A. Appraisal and assessment of world water resources. *Water Int.* **2000**, *25*, 11–32. [[CrossRef](#)]
69. Palhares, J. Consumo de água na produção animal. In *Embrapa Pecuária Sudeste-Comun. Técnico (Infoteca-E)*; Embrapa Pecuária Sudeste: São Carlos, SP, Brazil, 2013.
70. Ward, D.; McKague, K. *Water Requirements of Livestock*; Order No. 07-023; Ministry of Agriculture, Food and Rural Affairs: Ontario, Canada, 2007.
71. Zimmermann, B.; Elsenbeer, H.; De Moraes, J.M. The influence of land-use changes on soil hydraulic properties: Implications for runoff generation. *For. Ecol. Manag.* **2006**, *222*, 29–38. [[CrossRef](#)]
72. Germer, S.; Neill, C.; Krusche, A.V.; Elsenbeer, H. Influence of land-use change on near-surface hydrological processes: Undisturbed forest to pasture. *J. Hydrol.* **2010**, *380*, 473–480. [[CrossRef](#)]
73. Neill, C.; Jankowski, K.; Brando, P.M.; Coe, M.T.; Deegan, L.A.; Macedo, M.N.; Riskin, S.H.; Porder, S.; Elsenbeer, H.; Krusche, A.V. Surprisingly modest water quality impacts from expansion and intensification of large-scale commercial agriculture in the Brazilian Amazon-Cerrado region. *Trop. Conserv. Sci.* **2017**, *10*, 1–5.
74. Johnson, M.S.; Lehmann, J.; Couto, E.G.; Novaes Filho, J.P.; Riha, S.J. DOC and DIC in flowpaths of Amazonian headwater catchments with hydrologically contrasting soils. *Biogeochemistry* **2006**, *81*, 45–57. [[CrossRef](#)]
75. Xu, N.; Saiers, J.E. Temperature and hydrologic controls on dissolved organic matter mobilization and transport within a forest topsoil. *Environ. Sci. Technol.* **2010**, *44*, 5423–5429. [[CrossRef](#)] [[PubMed](#)]
76. Mann, P.; Davydova, A.; Zimov, N.; Spencer, R.; Davydov, S.; Bulygina, E.; Zimov, S.; Holmes, R. Controls on the composition and lability of dissolved organic matter in Siberia's Kolyma river basin. *J. Geophys. Res. Biogeosci.* **2012**, *117*. [[CrossRef](#)]
77. Lambert, T.; Darchambeau, F.; Bouillon, S.; Alhou, B.; Mbega, J.-D.; Teodoru, C.R.; Nyoni, F.C.; Massicotte, P.; Borges, A.V. Landscape control on the spatial and temporal variability of chromophoric dissolved organic matter and dissolved organic carbon in large African rivers. *Ecosystems* **2015**, *18*, 1224–1239. [[CrossRef](#)]
78. Wilson, H.F.; Xenopoulos, M.A. Effects of agricultural land use on the composition of fluvial dissolved organic matter. *Nat. Geosci.* **2009**, *2*, 37–41. [[CrossRef](#)]
79. Meyer, J.L.; Tate, C.M. The effects of watershed disturbance on dissolved organic carbon dynamics of a stream. *Ecology* **1983**, *64*, 33–44. [[CrossRef](#)]
80. Cammack, W.L.; Kalff, J.; Prairie, Y.T.; Smith, E.M. Fluorescent dissolved organic matter in lakes: Relationships with heterotrophic metabolism. *Limnol. Oceanogr.* **2004**, *49*, 2034–2045. [[CrossRef](#)]
81. Balcarczyk, K.L.; Jones Jr., J.; Jaffé, R.; Maie, N. Dissolved Organic Matter Bioavailability and Composition in Streams Draining Catchments with Discontinuous Permafrost. Doctoral Dissertation, University of Alaska Fairbanks, Fairbanks, AK, USA, 2008.
82. Baker, A.; Spencer, R.G. Characterization of dissolved organic matter from source to sea using fluorescence and absorbance spectroscopy. *Sci. Total Environ.* **2004**, *333*, 217–232. [[CrossRef](#)] [[PubMed](#)]
83. Hudson, N.; Baker, A.; Reynolds, D. Fluorescence analysis of dissolved organic matter in natural, waste and polluted waters—A review. *River Res. Appl.* **2007**, *23*, 631–649. [[CrossRef](#)]
84. Maie, N.; Scully, N.M.; Pisani, O.; Jaffé, R. Composition of a protein-like fluorophore of dissolved organic matter in coastal wetland and estuarine ecosystems. *Water Res.* **2007**, *41*, 563–570. [[CrossRef](#)] [[PubMed](#)]

85. Moran, M.A.; Zepp, R.G. Invited review role of photoreactions in the formation of biologically labile compounds from dissolved organic matter. *Oceanography* **1997**, *42*, 1307–1316.
86. Ishii, S.K.; Boyer, T.H. Behavior of reoccurring parafac components in fluorescent dissolved organic matter in natural and engineered systems: A critical review. *Environ. Sci. Technol.* **2012**, *46*, 2006–2017. [[CrossRef](#)] [[PubMed](#)]



© 2019 by the authors. Licensee MDPI, Basel, Switzerland. This article is an open access article distributed under the terms and conditions of the Creative Commons Attribution (CC BY) license (<http://creativecommons.org/licenses/by/4.0/>).